Article

Tuning of the Size of DyO Nanoparticles for Optimal Performance as an MRI Contrast Agent

Ma#gorzata Norek, Erik Kampert, Uli Zeitler, and Joop A. Peters

J. Am. Chem. Soc., **2008**, 130 (15), 5335-5340 • DOI: 10.1021/ja711492y • Publication Date (Web): 20 March 2008

J|A|C|S
ARTICLES

Published on Web 03/20/2008

Tuning of the Size of Dy_2O_3 Nanoparticles for Optimal Performance as an MRI Contrast Agent

Małgorzata Norek,[†] Erik Kampert,[‡] Uli Zeitler,[‡] and Joop A. Peters*,[†]

Biocatalysis and Organic Chemistry, Department of Biotechnology, Delft University of Technology, Julianalaan 136, 2628 BL Delft, The Netherlands; High Field Magnet Laboratory (HFML), Radboud University, P.O. Box 9010, 6500 GL Nijmegen, The Netherlands

Received December 31, 2007; E-mail: J.A.Peters@tnw.tudelft.nl

Abstract: The transverse ^{1}H relaxivities of aqueous colloidal solutions of dextran coated Dy_2O_3 nanoparticles of different sizes were investigated at magnetic field strengths (B) between 7 and 17.6 T. The particle size with the maximum relaxivity (r_2) appears to vary between 70 nm at 7 T ($r_2 \approx 190$ s^{-1} mM^{-1}) and 60 nm at 17.6 T ($r_2 \approx 675$ s^{-1} mM^{-1}). A small difference between r_2 and r_2^* was observed, which was ascribed to the effect of the dextran coating. The value of r_2 is proportional to B^2 up to 12 T after which it saturates. Independent magnetization measurements on these particles at room temperature at magnetic field strengths up to 30 T, however, show a typical paramagnetic behavior with a magnetization of the particle that is proportional to the field strength. The saturation in the curve of r_2 as a function of B^2 was tentatively explained by the presence of an extremely fast relaxing component of the signal at high field strengths, which is not observable on the NMR time scale. The results of this study can be exploited for the rational design of MRI contrast agents, based on lanthanide oxide particles, with high efficiencies at magnetic field strengths of more than 1.5 T.

Introduction

The present trend in magnetic resonance imaging (MRI) to move toward higher magnetic fields (>1.5 T) has led to an improvement of the spatial resolution and the contrast to noise ratio of the images. However, in molecular imaging, where cellular molecular events involved in normal and pathological processes are studied, the sensitivity of MRI is still an important issue.[1–3] Relatively high concentrations of contrast agents (CAs) have to be applied to achieve the desired contrast.[4,5] A possible way to overcome this problem is to apply particles conjugated to targeting moieties, which can bring a high payload of paramagnetic compound to the sites of interest.[6–9] At present, the most commonly used CAs are enhancing the longitudinal relaxation rate of water resulting in positive contrast (bright spots). At magnetic fields higher than 1 T the efficiency of these agents expressed as the relaxivity r_1 (the longitudinal relaxation rate enhancement per mM concentration of lanthanide ions) drops significantly. Since positive (r_1) CAs require direct interaction of the paramagnetic ion with water, the ability of magnetic nanoparticles to induce water proton relaxation enhancement is limited mainly to the water molecules that interact with the ions at the surface of the particles. Liposomal particulates with Gd^{3+} chelates incorporated in the surface have been shown to have a relaxivity that is invariant above a certain minimum vesicle diameter due to local fluctuations, which dominate the rotational correlation time.[10] For solid particles, however, in general a decrease in longitudinal relaxivity is observed upon increase of the particle size, due to the corresponding decrease of the surface-to-volume ratio.[11] Alternatively, high relaxivities can be achieved by susceptibility, negative (r_2), CAs. They reduce the phase coherence of water protons diffusing near their surface to an extent depending on the induced magnetic moment of these particles (or the magnetization of a single particle, M_p). The effect depends on the total number of paramagnetic ions per particle, the magnitude of the magnetic moment of the individual ion and the potential cooperative effect that enlarges the magnetic moment for the group to be larger than the sum of the moments of the individual

[†] Biocatalysis and Organic Chemistry, Delft University of Technology.
[‡] High Field Magnet Laboratory (HFML), Radboud University.

(1) Bowen, C. V.; Zhang, X.; Saab, G.; Gareau, P. J.; Rutt, B. K. *Magn. Reson. Med.* **2002**, *48*, 52–61.
(2) Foster-Gareau, P.; Heyn, Ch.; Alejski, A.; Rutt, B. K. *Magn. Reson. Med.* **2003**, *49*, 968–971.
(3) (a) Heyn, Ch.; Bowen, Ch. V.; Rutt, B. K.; Foster, P. J. *Magn. Reson. Med.* **2005**, *53*, 312–320. (b) Weissleder, R.; Mahmood, U. *Radiology* **2001**, *219*, 316–333.
(4) Massoud, T. F.; Gambhir, S. S. *Genes Dev.* **2003**, *17*, 545–580.
(5) Weissleder, R. *Radiology* **1999**, *212*, 609–614.
(6) Aime, S.; Cabella, C.; Colombatto, S.; Crich, S. G.; Gianolio, E.; Maggioni, F. *J. Magn. Reson. Imaging* **2002**, *16*, 394–406.
(7) Morawski, A. M.; Winter, P. M.; Crowder, K. C.; Caruthers, S. D.; Fuhrhop, R. W.; Scott, R. W.; Robertson, J. D.; Abendschein, D. R.; Lanza, G. M.; Wickline, S. A. *Magn. Reson. Med.* **2004**, *51*, 480–486.
(8) Norek, M.; Neves, I. C.; Peters, J. A. *Inorg. Chem.* **2007**, *46*, 6190–6196.
(9) Pereira, G. A.; Ananias, D.; Rocha, J.; Amaral, V. S.; Muller, R. N.; Vander Elst, L.; Tóth, É.; Peters, J. A.; Geraldes, C. F. G. C. *J. Mater. Chem* **2005**, *15*, 3832–3837.
(10) Tilcock, C.; Ahkong, Q. F.; Koenig, S. H; Brown, R. D.; Davis, M.; Kabalka, G .*Magn. Reson. Med.* **1992**, *27*, 44–51.
(11) Na, H. B.; Lee, J. H.; An, K.; Park, Y. I.; Park, M.; Lee, I. S.; Nam, D.-H.; Kim, S. T.; Kim, S.-H.; Kim, S.-W.; Lim, K.-H.; Kim, K.-S.; Kim, S.-O.; Hyeon, T. *Angew. Chem., Int. Ed.* **2007**, *46*, 5397–5401.
(12) Tromsdorf, U. I.; Bigall, N. C.; Kaul, M. G.; Bruns, O. T.; Nikolic, M. S.; Mollwitz, B.; Sperling, R. A.; Reimer, R.; Hohenberg, H.; Parak, W. J.; Förster, S.; Beisiegel, U.; Adam, G.; Weller, H. *Nano Lett.* **2007**, *7*, 2422–2427.

ions. Thus, r_2 increases with the magnetic field strength, B, and the particle size.[12] Recently this has been demonstrated in a study on cell labeling, where larger magnetic particles appear to be more efficacious.[13] Thanks to both the increased sensitivity of MRI and of the r_2 contrast agents at higher magnetic fields, the required dose is significantly lower than at low field; at 11.7 T the minimal concentration of negative CAs for satisfactory contrast enhancement is around 10 times lower than that at 1.5 T.[14] On the contrary, a model to assess the minimum concentration of r_1 CAs predicts not such a substantial increase in contrast upon increase of magnetic field strength.[15] All these features seem to make paramagnetic particles the ideal candidates for negative contrast agents at higher magnetic fields.

Previously, we have studied the transverse relaxivity of aqueous suspensions of lanthanide oxide nanoparticles in the presence of xanthan as an emulsifier.[16] The relaxivity appeared to be proportional to the magnetic field strength and to the square of the effective moment of the lanthanide, and cooperative effects between the individual ions of a particle do not occur. The xanthan was adsorbed in a thick layer on the surface of the particle. In this layer the water molecules were r_2 silent. The model that could explain these data suggests that the value of r_2 as a function of the particle size should have an optimum.[17–22]

Here, we report on a study of the effect of the particle size on the transverse relaxivity of aqueous suspensions of dextran coated dysprosium oxide particles, with the aim to determine the optimal radius. We focused on dysprosium oxide particles, because Dy^{3+} (together with holmium) has the highest effective moment among the lanthanides and thus the highest relaxivities. The values of magnetization of the Dy_2O_3 particles were determined independently by magnetization measurement and compared with the values as determined from the transverse relaxivity data.

Experimental Section

A suspension of nanoparticles with a particle size of 67 nm was obtained from Aldrich. This suspension was stabilized by an emulsifier not disclosed by the supplier and was used without further treatments.

Nanoparticles with average core radii of 37, 43, 59, and 95 nm were prepared starting from dysprosium oxide nanoparticles purchased from Aldrich (two different batches), which had a diameter of less than 40 nm as determined with XRD by the supplier. Previous TEM measurements have shown that these particles form spherical agglomerates consisting of nanosized plates with a size of 5–10 nm.[16] These particles were separated into fractions with various particle sizes by using centrifugation and filtration procedures.

Particles with an average radius of 37, 43, 59, 95 nm in the magnetic core were prepared via separation from two different batches of the commercially available nanopowder (0.1 g of Dy_2O_3 nanopowder dispersed in 100 mL of double distilled water) by using both centrifugation (4000 rpm for 10 min) and filtration of aqueous suspensions (syringe hydrophilic filters, the pore size of 0.2 μm).

The nanoparticles obtained were encapsulated in a dextran shell using the following procedure: 0.2 g of dextran (60–100 kD, purchased from Acros Organics, Geel, Belgium) was added to 10 mL of an aqueous suspension containing 4.3, 0.9, 6.2, 5.2 mg of Dy_2O_3 nanoparticles of radius of 37, 43, 59, and 95 nm, respectively, and then the mixture was stirred overnight at room temperature. The nanoparticles were subjected to ultrafiltration over a 100 kD filter and washed with six portions of 50 mL of double distilled water to remove unadsorbed dextran and other impurities. Cross-linking of the adsorbed dextran was achieved by suspending an amount of nanoparticles equivalent with 12 mmol Dy^{3+} in 100 mL of 5 M NaOH, and 40 mL of distilled water. To this suspension was added 40 mL of epichlorohydrin.[23] The mixture was incubated at room temperature for about 24 h with shaking to promote interaction of organic phase (epichlorohydrin) and aqueous phase, which contains the dextran-covered colloid.

The particles with an average radius of 1 nm were synthesized in diethylene glycol (DEG) according to a method described in the literature.[24] To a colloidal solution of 14.5 mg of the 1 nm Dy_2O_3 in 10 mL of DEG, was added a solution of 0.1 g of dextran in 10 mL of water. After stirring overnight at room temperature, the particles were filtered over a 100 kDa filter, washed with 10 portions of 50 mL of double distilled water, and immediately taken up in 5 mL of water. Finally, cross-linking with epichlorohydrin was performed using the procedure described above. The final purification of all samples was accomplished by ultrafiltration over a 100 kDa filter and washing of the residue with double distilled water (six times with 50 mL). The obtained colloidal solutions were diluted to a Dy^{3+} concentration of 0.25 mM, which is equivalent to a volume fraction of the particles, ν, of 5.97×10^{-6}. For the measurements at $B = 11.9$ and 17.6 T, the samples were further diluted to a concentration of 0.05 mM ($\nu \approx 1.2. \times 10^{-6}$), to increase the accuracy of the measured transverse relaxation times. The obtained aqueous colloidal solutions were highly stable; after several months still no precipitation was observed, whereas the DLS analyses and the relaxivities reported appeared to be reproducible after that time.

Water proton transverse relaxation times, T_2, were measured at 300 MHz (Varian-INOVA spectrometer), 400 MHz (Varian VXR-400 S spectrometer), 500 MHz (Bruker DRX 500 NMR spectrometer), and 750 MHz (Bruker DMX-750 NMR spectrometer) using the Carr−Purcell−Meiboom−Gill pulse sequence (CPMG). The values of T_2^* were evaluated from the linewidths. All experimental values of relaxation rates were corrected for diamagnetic contributions of pure water (0.5 s^{-1}).

The magnetization $M_p(B)$ of aqueous colloidal solutions of Dy_2O_3 nanoparticles were measured at the High Field Magnet Laboratory (HFML) in Nijmegen using a ballistic magnetization setup, running up to $B = 30$ T.

The dynamic light scattering (DLS) was performed with a DLS/SLS/ALV-5000 apparatus using a 35 mW HeNe laser with a wavelength of 633 nm. The intensity autocorrelation function was measured at an angle of 90° and analyzed with the CONTIN method. All samples were placed in an ultrasonic bath and were centrifuged prior to the DLS measurements in order to remove dust and other contaminants.

(13) Hsiao, J.-K.; Tai, M.-F.; Yang, Ch.-Y.; Chen, S.-T.; Wang, J.-L.; Ku, H.-Ch.; Liu, H.-M. *IEEE Trans. Magn.* **2007**, *43*, 2421–2423.
(14) Mills, P. H.; Ahrens, E. T. *Magn. Reson. Med.* **2007**, *57*, 442–447.
(15) Ahrens, E. T.; Rothbächer, U.; Jacobs, R. E.; Fraser, S. E.; *Proc. Natl. Acad. Sci. U.S.A.* **1998**, *95*, 8443–8448.
(16) Norek, M.; Pereira, G. A.; Geraldes, C. F. G. C.; Denkova, A.; Zhou, W.; Peters, J. A. *J. Phys. Chem. C* **2007**, *111*, 10240–10246.
(17) Hardy, P. A.; Henkelman, R. M. *Magn. Reson. Imaging* **1989**, *7*, 265–275.
(18) Koenig, S. H. *Invest. Radiol.,* **1998**, *11*, 822–827.
(19) Weisskoff, R. M.; Zuo, C. S.; Boxerman, J. L.; Rosen, B. R. *Magn. Reson. Med.* **1994**, *31*, 601–610.
(20) Yung, K.-T. *Magn. Reson. Imag.,* **2003**, *21*, 451–463.
(21) Gillis, P.; Moiny, F.; Brooks, R. A. *Magn. Reson. Med.* **2002**, *47*, 257–263.
(22) (a) Muller, R. N.; Gillis, P.; Moiny, F.; Roch, A. *Magn. Reson. Med.* **1991**, *22*, 178–182. (b) Hardy, P. A.; Henkelman, R. M. *Magn. Reson. Imaging* **1989**, *7*, 265–275.
(23) Palmacci, S.; Josephson, L.; 1993, U.S. Patent 5,262,176.
(24) Bridot, J.-L.; Faure, A.-Ch.; Laurent, S.; Rivière, Ch.; Billotey, C.; Hiba, B.; Janier, M.; Josserand, V.; Coll, J.-L.; Vander Elst, L.; Muller, R.; Roux, S.; Perriat, P.; Tillement, O. *J. Am. Chem. Soc.* **2007**, *129*, 5076–5084.

Table 1. Average Particle Radii before and after Coating with Dextran (nm) as Determined by DLS of the Particles Used in this Study and the Effective Radii As Determined from the Transverse Relaxivities

before coating	after coating	r_{diff}[b]
1	20	5 (±1.5)
37	75	56 (±14)
43	94	59 (±15)
59	67	61 (±5)
67[a]	–	–
95	139	–

[a] Commercially available suspension containing unknown emulsifier. [b] See text.

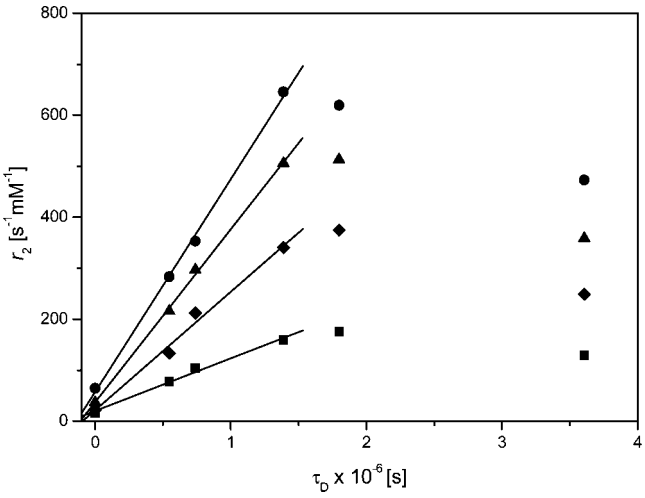

Figure 1. Transverse relaxivity r_2 as a function of the estimated diffusion correlation time τ_D ($\tau_D = r_c^2/D$) of dextran coated Dy_2O_3 nanoparticles suspended in water at 25 °C, at magnetic fields $B = 7$ (squares), 9.4 (diamonds), 11.9 (triangles), and 17.6 T (circles). The values of r_2 are averages of the four measurements for τ_{CP} ranging between 1 – 5 ms (the inaccuracy of r_2 values is 3–10%). The linear curves are fits of eq 4 to the experimental points (correlation coefficients 0.99512, 0.99448, 0.99844, and 0.99919, respectively).

The concentrations of Dy^{3+} in the samples were determined from the bulk magnetic susceptibility shift (BMS) by using a previously described procedure.[25]

Results and Discussion

The DLS analyses of the particles studied (see Supporting Information, Figure S1) show that the particles are characterized by a narrow size distribution both before and after dextran coating. The data obtained are summarized in Table 1.

The R_2 values obtained with CPMG measurements were independent of the time interval between two refocusing pulses (τ_{CP}) for the range of τ_{CP} values applied in this study (0.5–5 ms, see Supporting Information Figure S2). The transverse relaxivity r_2 (the transverse relaxation rate enhancement of protons by the particles expressed per mM concentration of Dy^{3+}) is strongly dependent on the size of Dy_2O_3 nanoparticles, as reflected in Figure 1, showing r_2 as a function of the diffusion correlation time τ_D ($\tau_D = r_c^2/D$, where r_c is the radius of the Dy_2O_3 core of the particle, $D = 2.5 \times 10^{-9}$ m^2 s^{-1} is the diffusion coefficient of water at 25 °C).

In general, r_2 relaxivity has contributions triggered by two correlation times: the diffusion correlation time, τ_D, and the static correlation time, $1/\Delta\omega$ (where $\Delta\omega$ is the difference in Larmor frequency at the particle surface and that at infinity).[20] The latter correlation time is dependent only on magnetic properties of the particle, not upon its size. The relaxation behavior as shown in Figure 1 is characteristic for aqueous suspensions of magnetic particles, when the relaxivity is governed by the diffusion relaxation mechanism. The data show that two regimes can be distinguished.[17–22] In the first regime, relevant for small particle sizes ($\tau_D < 1.5 \times 10^{-6}$ s), the condition for motional narrowing is satisfied, which implies that diffusion phenomena are faster than the spatial variation of the local field inhomogeneities produced by a single particle ($\tau_D << 1/\Delta\omega$), and r_2 increases linearly with τ_D. The relaxivity then is described in terms of the outer-sphere theory (OS).[26] Upon increase of the particle size, τ_D becomes comparable with $1/\Delta\omega$, and upon further increase of τ_D, the second regime is reached, where r_2 decreases with τ_D ($\tau_D > 1.5 \times 10^{-6}$ s in Figure 1). Figure 1 shows that maximum relaxivity at 7 T is obtained for Dy_2O_3 nanoparticles with a radius of about 70 nm, whereas at $B = 17.6$ T, the maximum relaxivity is reached at a radius of 60 nm.

In principle, a third regime should exist for very large particles ($\tau_D >> 1/\Delta\omega$). Then, the diffusion can be practically neglected and the relaxation rate is solely dependent on $\Delta\omega$ and the number of spheres (as reflected in the volume fraction, ν). The concerning relaxivity mechanism is described by the static dephasing regime theory (SDR).[27–29] However, this regime is not observed for the particles investigated in this study.

The Larmor frequency shift $\Delta\omega$, is given by eq 1, where M_p is the induced magnetic moment of a particle, and γ is the proton gyromagnetic ratio. M_p can be expressed as in eq 2.[30]

$$\Delta\omega = \gamma M_p/3 \tag{1}$$

$$M_p = \frac{n}{v}\mu_0\mu_C \tag{2}$$

$$\mu_C = \frac{\mu_{eff}^2 B}{3kT}, \quad \text{where } \mu_{eff} = g\mu_B\sqrt{J(J+1)} \tag{3}$$

Here n is the number of Ln^{3+} ions per particle, v is the volume of a single particle, μ_0 the vacuum magnetic permeability, and μ_C the Curie moment. The latter is given by eq 3, where μ_B is the Bohr magneton, g the Landé g-factor, J the quantum number of the total spin, k the Boltzmann constant, and T the absolute temperature.

Provided that $\tau_D << 1/\Delta\omega$ and that the diffusion correlation time is not disturbed by the refocusing pulses separated by τ_{CP} ($\tau_D << \tau_{CP}$), the relaxivity of water protons can be described by eq 4:[31,32]

$$R_2 = R_2^0 + \frac{1}{2}\Delta\omega^2\nu\tau_D \tag{4}$$

Here, R_2^0 is the contribution due to diamagnetic relaxation. Therefore, the slopes of the initial linear part of the curves in Figure 1 are given by $\frac{1}{2}\Delta\omega^2 v$. The values of $\Delta\omega$ as calculated from these slopes are given as a function of B in Figure 2. It

(25) Corsi, D. M.; Platas-Iglesias, C.; van Bekkum, H.; Peters, J. A. *Magn. Reson. Chem.* **2001**, *39*, 723–726.
(26) Brooks, R. A.; Moiny, F.; Gillis, P. *Magn. Reson. Med.* **2001**, *45*, 1014–1020.
(27) Brown, R. J. S. *Phys. Rev.* **1961**, *121*, 1379–1382.
(28) Yablonskiy, D. A.; Haacke, E. M. *Magn. Reson. Med.* **1994**, *32*, 749–763.
(29) Yablonskiy, D. A.; Haacke, E. M. *Magn. Reson. Med.* **1997**, *37*, 872–876.
(30) Roch, A.; Gossuin, Y.; Muller, R. N.; Gillis, P. *J. Magn. Magn. Mater.* **2005**, *293*, 532–539.
(31) Jensen, J. H.; Chandra, R. *Magn. Reson. Med.* **2000**, *44*, 144–156.
(32) Jensen, J. H.; Chandra, R. *Magn. Reson. Med.* **2000**, *43*, 226–236.

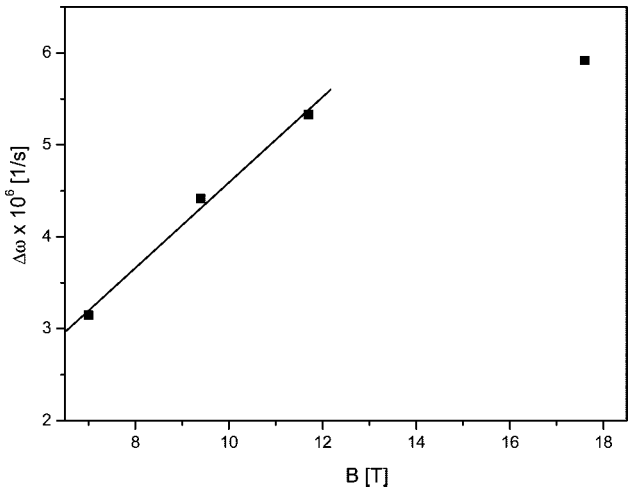

Figure 2. $\Delta\omega(B)$ relation for dextran-coated Dy_2O_3 nanoparticles as determined from the fit of eq 4 to the experimental points presented in Figure 1 ($R = 0.9945$).

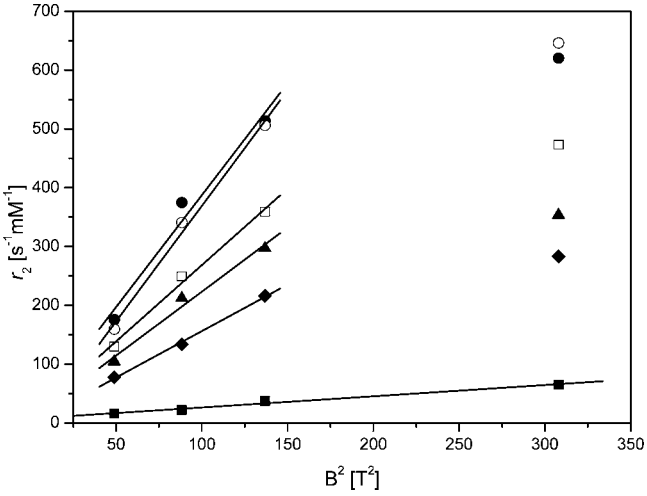

Figure 3. The transverse relaxivity, r_2, as a function of B^2 for dextran-coated Dy_2O_3 nanoparticles; the curves are the linear fits to the experimental points for the nanoparticles with core radii of 1 nm (squares, $R = 0.99198$), 37 nm (diamonds, $R = 0.99881$), 43 nm (triangles, $R = 0.99171$), 59 nm (open circles, $R = 0.99621$), 67 nm (filled circles, $R = 0.9868$) and 95 nm (open squares, $R = 0.99645$).

can be seen that the Larmor frequency shift is linearly dependent on B up to a magnetic field strength of about 12 T, which is in agreement with eqs 1−3, but at $B > 12$ T, the linear relationship breaks. Furthermore, according to eq 4, r_2 should increase with B^2. This expectation seems to be fulfilled only for the sample with particles with a core radius of 1 nm. For samples containing larger magnetic particles, at $B \approx 12$ T, the curve $r_2(B^2)$ flattens (Figure 3).

A possible explanation for this behavior is that at high magnetic fields saturation of M_p may occur, which is not likely for paramagnetic compounds. However, magnetization measurements of Gd_2O_3 nanoparticles both coated with dextran and uncoated, have shown a significant difference in the $M_p(B)$ curves. The results have suggested that upon coating, Gd_2O_3 particles become superparamagnetic.[33] To clarify this issue, the M_p values of the Dy_2O_3 particles were determined independently by magnetization measurements at high magnetic fields. As

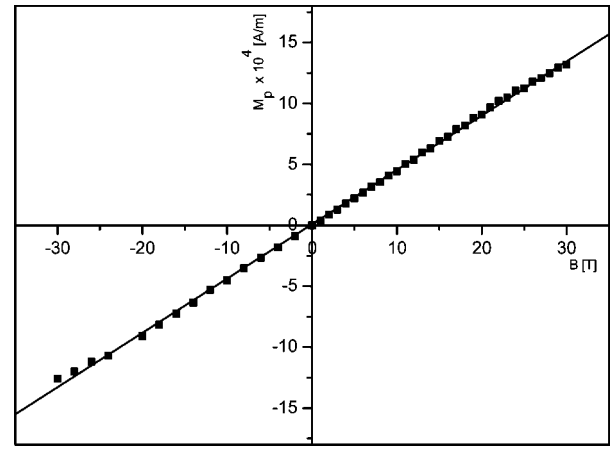

Figure 4. The magnetization measurement $M_p(B)$ for dextran-coated Dy_2O_3 nanoparticles (the data refers to the dextran-coated particles with a core size $r_c = 59$ nm at room temperature ($R = 0.99667$).

expected, at room temperature the data show a typical paramagnetic behavior up to the $B = 30$ T (Figure 4). Furthermore, no effect of dextran coating on the measured M_p was detected.

Therefore, saturation of magnetization of a single particle M_p must be ruled out as a reason for the saturation of $\Delta\omega$, and consequently also of r_2, at relatively high magnetic fields. Most likely at those high magnetic field strengths, the protons in close proximity of the magnetic particles have extremely fast signal decay and are not observable on the NMR time scale. If so, the r_2 relaxivity measurement gives underestimated values of M_p. This effect can be rationalized by the increase of M_p and thus the increase of $\Delta\omega$ upon increase of B. The diffusion correlation time τ_D, at $B > 12$ T, becomes much larger than the static correlation time $1/\Delta\omega$; at $B = 17.6$ T, the difference is an order of magnitude. Therefore, for the protons present in the area, where the local field inhomogeneities are the largest, the condition $\tau_D >> 1/\Delta\omega$ is operative, resulting in very inefficient averaging out of the spin phases of these protons by diffusion. Consequently, they are not included in the magnetization pool, and a larger T_2 is measured with the CPMG pulse sequence.

The aqueous colloidal solution of dextran-coated 1 nm Dy_2O_3 nanoparticles, with τ_D of 4×10^{-10} s, behaves slightly differently, as far as the $r_2(B^2)$ relation is concerned (see Figure 3). Due to the extremely fast diffusion of these particles, the local field inhomogeneities are very efficiently smoothened out, resulting in a relatively slow relaxation process of water protons (T_2 is relatively long) even at high B. Accordingly, there is no loss of NMR signal, and therefore, the r_2 of these particles is proportional to B^2 for all magnetic field strengths applied.

The experimental results show that the magnetization values, as determined from the relaxivity r_2 data by the use of eqs 1 and 4, are in a good agreement with those determined with the direct magnetization measurement (see Figure 5), at magnetic fields lower than 12 T. The CPMG method is known to be very sensitive to the diffusion phenomena. Therefore, the values of r_2 can vary, depending on the source and the extent to which the diffusion process is disturbed. For this reason, we decided to compare the directly measured magnetization data with the magnetizations calculated from r_2^* determined from line widths. The latter data represent the maximal, possible, relaxivity of the water protons and are not disturbed by diffusion effects.[28]

The values of the both r_2^* and r_2 for the various nanoparticles are shown in Figure 6. The two regimes mentioned above (one where the condition $\tau_D << 1/\Delta\omega$ holds, and the other, where

(33) McDonald, M. A.; Watkin, K. L. *Acad. Radiol.* **2006**, *13*, 421–427.

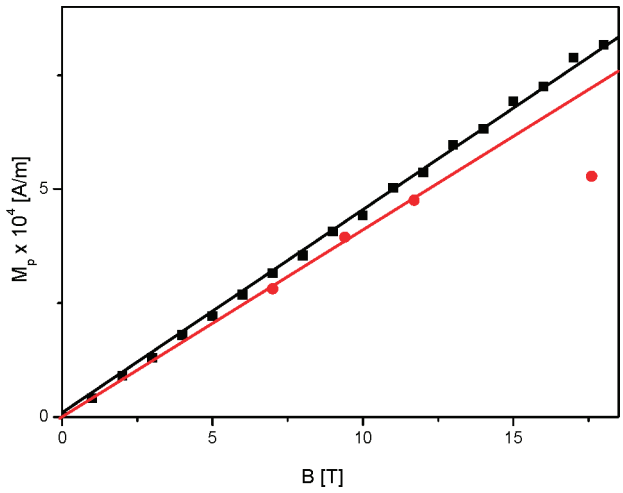

Figure 5. Comparison of M_p of Dy_2O_3 nanoparticles as determined from the relaxivity r_2 with the use of eqs 1 and 4 (circles in red, the curve represents a linear fit to the first three points at $B = 7$, 9.4, 11.9 T with $R = 0.99667$) with the results of the magnetization measurement (squares, black curve represents the linear fit to the data with $R = 0.99951$).

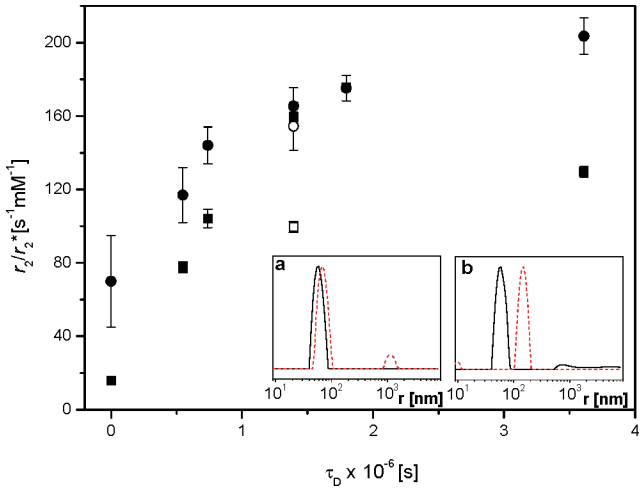

Figure 6. r_2/r_2^* (r_2 squares, r_2^* circles) as a function of τ_D for dextran-coated Dy_2O_3 nanoparticles at $B = 7$ T and room temperature. The insets show the DLS pictures of dextran-coated 59 nm Dy_2O_3 nanoparticles (core - solid-black curve; the coated particles - dashed-red curve). Empty symbols correspond to the particles of 59 nm with the coating of around 100 nm (inset b), as compared to the same particles (the same τ_D with filled symbols), but with a dextran layer of ~10 nm (inset a).

the opposite is operative), are also reflected in the curve of r_2^* as a function of τ_D. Similar to r_2, r_2^* is increasing linearly with τ_D for relatively small sizes of particles ($\tau_D < 10^{-6}$ s), and for larger radii, r_2^* seems to saturate at a constant value, whereas r_2 decreases with τ_D. According to the outer—sphere theory, r_2^* and r_2 should be equal under the condition $\tau_D << 1/\Delta\omega$, which in the present study is fulfilled for $\tau_D < 1.5 \times 10^{-6}$ s.[18,19] However, the experimental data show that for most samples r_2^* is larger than r_2, even for very small τ_D values. The slope of the initial linear part of the curve for r_2^* is comparable with the slope of the curve for the corresponding r_2 values. We ascribe this relaxation "loss" to the protons within the dextran layer. This is strongly supported by the data for a sample of a commercially available aqueous suspension of Dy_2O_3 nanoparticles, which had an average particle size of 67 nm and no coating, and showed equal values for r_2^* and r_2. Moreover, the ratio r_2^*/r_2 for a sample of the particles with a core of 59 nm coated with a relatively thick dextran layer of about 100 nm (Figure 6, inset b), appeared to be around 2 times higher than that for the same particles but covered with a dextran layer of only about 10 nm (Figure 6, inset a).

The data also demonstrate that the gap between r_2^* and r_2 increases with the thickness of the coating. The maximum value of r_2 is reached when it is equal to r_2^*, and there, the thickness of the coating should not exceed 10 nm. This phenomenon can be explained by considering water molecules in the dextran layer as being governed by the static dephasing regime (SDR). Most probably due to the formation of hydrogen bonds with dextran, the water molecules are hindered to move freely within the time interval between the two refocusing pulses of the CPMG pulse sequence. As an effect, the dephasing there is fully recovered after these pulses and then $r_2 \approx 0$.[16]

To estimate the thickness of the layer, where the protons are fully refocused by the π pulses, we define a sphere around the particle with radius r_{diff}, within which the protons do not contribute to the overall transverse relaxivity. This sphere includes the part of the cross-linked dextran coating that is not permeable by water and the water protons around the core of which the dephasing of the magnetization is fully refocused. Then $\Delta\omega$, τ_D, and v can be scaled as in eqs 6–8.

$$\Delta\omega_{diff} = \Delta\omega\left(\frac{r_c}{r_{diff}}\right)^3 \tag{6}$$

$$\tau_{D,diff} = \tau_D\left(\frac{r_{diff}}{r_c}\right)^2 \tag{7}$$

$$v_{diff} = v\left(\frac{r_{diff}}{r_c}\right)^3 \tag{8}$$

Equation (4) can then be rewritten as:

$$R_2 = R_2^0 + \frac{1}{2}\Delta\omega^2 v\tau_D\left(\frac{r_c}{r_{diff}}\right) \tag{9}$$

whereas R_2^* is given by eq (10).

$$R^* = R_2^{0*} + \frac{1}{2}\Delta\omega^2 v\tau_D \tag{10}$$

From the values of r_2 and r_2^* for $\tau_D \leq 10^{-6}$ s and eqs 6–10, values for r_{diff} were estimated. The results are included in Table 1. It can be seen that the value of r_{diff} is always smaller than the radius of the coated particles as measured by DLS. This suggests that the diffusion of water in the outer part of the dextran layer is not limited by hydrogen-bond formation with the dextran.

For the condition $\tau_D > 1/\Delta\omega$ ($\tau_D > 1.5 \times 10^{-6}$ s), represented in this study only by the largest particles (with $\tau_D = 3.6 \times 10^{-6}$ s), the difference between r_2^* and r_2 seems to be large, as would be expected from the OS model. However, in this case, still no increase of r_2 upon the increase of τ_{CP} was observed. This should be expected, since both diffusion correlation time and the dephasing time are still much shorter than τ_{CP} ($\tau_{CP} >> \tau_D$, $1/\Delta\omega$), and consequently, r_2 cannot reach r_2^*.[34]

Conclusion

The transverse relaxivity of dextran-coated particles is dependent on the particle radius. Optimum relaxivities are reached with particles having a core radius of about 70 nm. Under those

(34) Pereira, G. A.; Norek, M.; Peters, J. A.; Ananias, D.; Rocha, J.; Geraldes, C. F. G. C. *Dalton Trans.* **2008**, In press.

conditions the r_2 value is about 190 s^{-1} mM^{-1} at 7 T, and 25 °C, which is comparable with the relaxivity of, for example, PEGylated magnetoliposomes ($r_2 = 240$ s^{-1} mM^{-1}) or protein-coated magnetoferritin ($r_2 = 218$ s^{-1} mM^{-1}) at $B = 1.5$ T.[35] At even higher magnetic fields, the proton relaxivity r_2 in the presence of Dy_2O_3 nanoparticles is increasing with B^2, in contrast to superparamagnetic entities, which due to their constant magnetic moment, produce no r_2 enhancement at $B >$ 1.5 T. Dextran coating appeared to improve the colloidal stability of water suspensions of the particles. The relaxation behavior of the suspensions of the dextran-coated particles differs significantly from that of the previously studied uncoated particles in the presence of xanthan gum as an emulsifier. There, a huge gap between r_2^* and r_2 ($r_2^* \approx 6\ r_2$) was observed, whereas r_2 was dependent on τ_{CP} which is explained by the presence of the high molecular weight xanthan gum, forming a thick layer adsorbed on the particles surface. As a result, the effective radius of the magnetic entities (r_{diff}) was much larger than the real particle size. The relaxivities could be considered as the weighted contributions of protons within the xanthan layer, subjected to the SDR, and of the protons outside this layer, subjected to the motional narrowing regime. Since r_{diff} for the previously studied system was very large ($\sim$0.7 μm) as compared to r_{diff} for the presently studied dextran coated particles (2–19 nm), the weight of the SDR-dominated relaxation process was also relatively large. This resulted in linear-like dependence of r_2 on B. For the dextran-coated nanoparticles, the transverse relaxivity is predominantly affected by the motional narrowing regime and thus is proportional to B^2.

Dy_2O_3 nanoparticles, due to their excellent relaxometric properties, can provide the desired contrast agents for molecular imaging at high magnetic fields. The results of the present study can form the foundation for rational design of efficient MRI contrast agents based on coated lanthanide oxide particles; the present models will also be applicable to other types of coatings. The coatings can be functionalized anchoring groups for targeting vectors.[36–41] A Dy_2O_3 particle with optimal relaxivity has a radius of about 70 nm. Consequently, a targeting vector conjugated to such a particle can deliver about 10^7 Dy^{3+} ions, each with a relaxivity of 190 s^{-1} mM^{-1} at the site of interest. This should be sufficient for application in molecular imaging. It has been demonstrated already that the detection of a single tumor cell *in vivo* is feasible by MRI at 1.5 T.[42–44] It should be noted however, that various other factors are of importance for application in molecular imaging, including the toxicity, protection of the particle by the coating for leaching, and the effect of the particle size on the biodistribution. Further research to establish this is required.

After optimizing the spatial resolution and the contrast-to-noise ratio by application of higher magnetic fields, and improving the sensitivity of MRI by the use of CAs highly efficient at those strong fields, MRI will possibly offer the best solution for noninvasive molecular imaging. It would be of great interest to link the potential MRI imaging properties of lanthanide oxide nanoparticles with therapeutic applications.[45,46] Recently, it has been reported that holmium-containing particles can be used for the radionuclide therapy of cancer cells and the paramagnetic properties can be utilized for monitoring the therapy by means of MRI.[47] Since the magnitude of the magnetic moments of Ho and Dy are the same, it may be expected that the relaxation behavior of Ho- and Dy-containing particles are similar.

Acknowledgment. We thank Prof. Olivier Tillement, Brice Mutelet, Jean-Luc Bridot, of the University of LPCML - UMR 5620, Lyon 1 (France), for their kind help in the synthesis of 1 nm Dy_2O_3 nanoparticles, Johan Hollander from the Leiden Institute of Chemistry, Gorlaeus Laboratories, P.O. Box 9502, 2300 RA Leiden (The Netherlands) for his help in the relaxivity measurements at magnetic fields 11.9 and 17.6 T, and Antonia Denkova from the Laboratory of Physical Chemistry and Molecular Thermodynamics, Delft University of Technology, for her assistance in DLS measurements. Thanks are due to the EU for financial support *via* a Marie Curie training site host fellowship (QLK5-CT-2000-60062). This work was done in the frame of COST Action D38 "Metal-Based Systems for Molecular Imaging Applications "and the EU Network of Excellence European Molecular Imaging Laboratory" (EMIL, LSCH-2004-503569). Part of this work has been supported by EuroMagNET under EU Contract No. RII3-CT-2004-506239 and by the Stichting Fundamenteel Onderzoek der Materie (FOM) with financial support from the Nederlandse Organisatie voor Wetenschappelijk Onderzoek (NWO).

Supporting Information Available: DLS pictures of the particles studied and r_2 dependence on τ_{CP}. This material is available free of charge via the Internet at http://pubs.acs.org.

JA711492Y

(35) Mornet, S.; Vasseur, S.; Grasset, F.; Dugnet, E. *J. Mater. Chem.* **2004**, *14*, 2161–2175.
(36) Josephson, L.; Tung, Ch.-H.; Moore, A.; Weissleder, R. *Bioconjugate Chem.* **1999**, *10*, 188–191.
(37) Wagner, K.; Kautz, A.; Röder, M.; Schwalbe, M.; Pachmann, K.; Clement, J. H.; Schnabelrauch, M. *Appl. Organometal. Chem.* **2004**, *18*, 514–519.
(38) Petri-Fink, A.; Chastellain, M.; Juillerat-Jeanneret, L.; Ferrari, A.; Hofmann, H. *Biomaterials* **2005**, *26*, 2685–2694.
(39) Schulze, K.; Koch, A.; Schöpf; B.; Petri, A.; Steitz, B,; Chastellain, M.; Hofmann, M.; Hofmann, H.; Rechenberg, B. *J. Magn. Magn. Mater.* **2005**, *293*, 419–432.
(40) Tan, W. B.; Huang, N.; Zhang, Y. *J. Colloid Interface Sci.* **2007**, *320*, 464–470.
(41) Tan, W. B.; Zhang, Y. *J. Nanosci. Nanotechnol.* **2007**, *7*, 2389–2393.
(42) Muhlen von zur, C.; Elverfeldt von, D.; Bassler, N.; Neudorfer, I.; Steitz, B.; Petri-Fink, A.; Hofmann, H.; Bode, C.; Peter, K. *Atherosclerosis* **2007**, *193*, 102–111.
(43) Hilger, I.; Trost, R.; Reichenbach, J. R.; Linss, W.; Lisy, M.-R.; Berndt, A.; Kaiser, W. A. *Nanotechnology* **2007**, *18*, 135103.
(44) Shapiro, E. M.; Sharer, K.; Skrtic, S.; Koretsky, A. P. *Magn. Reson. Med.* **2006**, *55*, 242–249.
(45) Larson, T. A.; Bankson, J.; Aaron, J.; Sokolov, K. *Nanotechnology* **2007**, *18*, 325101.
(46) Ji, X.; Shao, R.; Elliott, A. M.; Stafford, R. J.; Esparza-Coss, E.; Bankson, J. A.; Liang, G.; Luo, Z.-P.; Park, K.; Markert, J. T.; Li, Ch. *J. Phys. Chem. C* **2007**, *111*, 6245–6251.
(47) Vente, M. A. D.; Hobbelink, M. G. G.; Van het Schip, A. D.; Zonnenberg, B. A.; Nijsen, J. F. W. *Anti-Cancer Agents Med. Chem.* **2007**, *7*, 441–459.